molecular pharmaceutics

Article

Cite This: Mol. Pharmaceutics 2019, 16, 3145−3156

pubs.acs.org/molecularpharmaceutics

Nanobody-Targeted Photodynamic Therapy Selectively Kills Viral GPCR-Expressing Glioblastoma Cells

Timo W. M. De Groof,[†,#] Vida Mashayekhi,[‡,#] Tian Shu Fan,[†] Nick D. Bergkamp,[†] Javier Sastre Toraño,[§] Jeffrey R. van Senten,[†] Raimond Heukers,[†,∥] Martine J. Smit,[*,†,∇] and Sabrina Oliveira[‡,⊥,∇]

[†]Division of Medicinal Chemistry, Amsterdam Institute for Molecules Medicines and Systems (AIMMS), Vrije Universiteit Amsterdam, De Boelelaan 1108, 1081 HZ Amsterdam, The Netherlands

[‡]Division of Cell Biology, Department of Biology, Utrecht University, 3584 CH Utrecht, The Netherlands

[§]Chemical Biology and Drug Discovery, Department of Pharmaceutical Sciences, Utrecht University, 3584 CG Utrecht, The Netherlands

[∥]QVQ B.V., Yalelaan 1, 3484 CL Utrecht, The Netherlands

[⊥]Pharmaceutics, Department of Pharmaceutical Sciences, Utrecht University, 3584 CG Utrecht, The Netherlands

Supporting Information

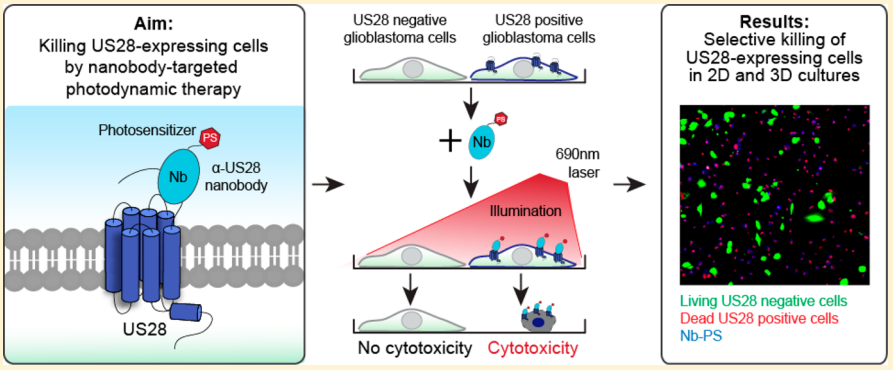

ABSTRACT: Photodynamic therapy (PDT) eradicates tumors by the local activation of a photosensitizer with near-infrared light. One of the aspects hampering the clinical use of PDT is the poor selectivity of the photosensitizer. To improve this, we have recently introduced a new approach for targeted PDT by conjugating photosensitizers to nanobodies. Diverse G protein-coupled receptors (GPCRs) show aberrant overexpression in tumors and are therefore interesting targets in cancer therapy. Here we show that GPCR-targeting nanobodies can be used in targeted PDT. We have developed a nanobody binding the extracellular side of the viral GPCR US28, which is detected in tumors like glioblastoma. The nanobody was site-directionally conjugated to the water-soluble photosensitizer IRDye700DX. This nanobody−photosensitizer conjugate selectively killed US28-expressing glioblastoma cells both in 2D and 3D cultures upon illumination with near-infrared light. This is the first example employing a GPCR as target for nanobody-directed PDT. With the emerging role of GPCRs in cancer, this data provides a new angle for exploiting this large family of receptors for targeted therapies.

KEYWORDS: *nanobody, photodynamic therapy, targeted photosensitizer, cancer, G protein-coupled receptors, glioblastoma, US28*

INTRODUCTION

Photodynamic therapy (PDT) is a minimally invasive modality where cancer cells are eradicated through local activation of a photosensitizer, by means of near-infrared light.[1] Activation of the photosensitizer leads to the production of singlet oxygen species, which have detrimental effects on proteins, lipids, and nucleic acids, resulting in cell toxicity, vascular responses, and additional inflammatory responses.[1] However, one of the main aspects hampering the use of PDT in the clinic is the hydrophobicity of the photosensitizer and its poor selectivity. This leads to off-target effects, the need to wait 2−4 days between administration of the photosensitizer and light application, and photosensitivity several weeks post PDT.[1,2] To improve this, more hydrophilic photosensitizers have been generated and/or other approaches like nanoparticles have been used for photosensitizer delivery.[3−5] In addition, photosensitizers have successfully been conjugated to antibod-

Received: March 29, 2019
Revised: May 29, 2019
Accepted: June 5, 2019
Published: June 5, 2019

ies directed against tumor antigens.[6,7] Currently, a phase I clinical study, involving the water-soluble photosensitizer IRDye700DX conjugated to an epidermal growth factor receptor (EGFR) targeting antibody is ongoing, for head and neck cancer.[8] The conjugation of a photosensitizer to monoclonal antibodies has increased the selectivity, showing promising results, but the large size of these antibody−photosensitizer conjugates impedes efficient tumor penetration and has slow clearance.[9−11] As an alternative, we have introduced nanobody-targeted PDT for more effective tumor penetration and faster clearance of the conjugates.[12,13]

Nanobodies are antibody-fragments derived from heavy-chain antibodies from Camelidae family members, which can be generated by immunization of llamas/alpacas with an antigen of interest.[14] Nanobodies display low immunogenicity, are highly soluble and physically stable, and have a 10-fold lower molecular weight (12−15 kDa), compared to conventional antibodies. This enables enhanced tumor penetration and the ability to bind cryptic antigenic sites inaccessible for conventional antibodies.[15−17] In previous studies, nanobodies targeting the epidermal growth factor receptor (EGFR) were successfully conjugated with the water-soluble photosensitizer IRDye700DX and used for targeted PDT *in vitro* and *in vivo* resulting in selective toxicity to EGFR-overexpressing tumor cells and extensive tumor damage.[12,13]

G protein-coupled receptors (GPCRs) are a family of receptors that play a prominent role in multiple physiological processes and are involved in multiple diseases, including cancer.[18−20] In several types of cancers, GPCR overexpression and/or dysregulated signaling contributes to angiogenesis, metastasis, and/or tumor growth.[21−23] These findings have led to an increasing interest in targeting GPCRs in cancer. To date, several GPCR-targeting nanobodies have already shown therapeutic potential in cancer, by inhibiting GPCR signaling.[24−29] Alternatively, such nanobodies could serve as ideal moieties for guiding functional groups, including photosensitizers, toward cancer cells.

Herpesviruses also contain genes encoding for GPCRs with high homology to human chemokine receptors. The human cytomegalovirus (HCMV) is a human herpesvirus with an estimated seroprevalence of approximately 50 to 90% of the worldwide population.[30,31] HCMV and US28, one of the four HCMV-encoded viral GPCRs, have been detected in multiple tumors, including gliomas, colorectal cancer, and prostate cancer.[32−38] In particular, US28 activates oncogenic signaling pathways and displays an oncomodulatory role in the progression of tumors like glioblastoma.[27,32,33,39−41] We recently developed an US28-targeting nanobody, which partially inhibits this US28-enhanced tumor growth *in vitro* and *in vivo* by inhibiting constitutive US28 signaling.[27] Since US28 is a foreign viral target expressed in tumors, but not in the surrounding healthy tissue, US28 would be an ideal target for selective therapies, including nanobody-targeted PDT.

The aim of this research was to eradicate US28-expressing glioblastoma cells using nanobody-targeted PDT. For this, we have selected a new nanobody that binds a discontinuous epitope of US28 with high affinity. We have conjugated the water-soluble photosensitizer IRDye700DX to an unpaired cysteine in a C-terminal tag of the nanobody without compromising the binding affinity. Notably, we were able to selectively kill US28-expressing glioblastoma cells in 2D cultures, as well as 3D spheroids. These findings show the potential of GPCR-targeting nanobodies in nanobody-directed PDT.

EXPERIMENTAL SECTION

DNA Constructs. The pVUN014 phagemid vector was a gift from Prof. Dr. H. J. de Haard (argenx BV, Zwijnaarde, Belgium). The pET28a vector for periplasmic production of nanobodies in *E. coli* was described previously.[42] The pcDEF3 vector was a gift from Dr. J. A. Langer.[43] Genes encoding the different US28 mutants (US28-Δ2-22) or isoforms (VHL/E, AD169, and TB40/E) were either described previously or were ordered from Eurofins (Ebersberg, Germany).[44]

Cell Culture. hek293t cells and U251 cells were purchased from ATCC (Wesel, Germany). Doxycycline-inducible US28 expression in U251 cells (U251-iUS28) and in HEK293T cells (HEK293T-iUS28) were described previously.[27] To induce US28 expression, cells were induced with doxycycline (1 μg/mL, D9891, Sigma-Aldrich, Saint Louis, Missouri, USA) for 48 h. Cells were grown at 5% CO_2 and 37 °C in Dulbecco's modified Eagle's medium (Thermo Fisher Scientific, Waltham, Massachusetts, USA) supplemented with 1% penicillin/streptomycin (Thermo Fisher Scientific) and 10% Fetal Bovine Serum (FBS, Thermo Fisher Scientific). FBS was heat inactivated (30 min, 60 °C) for the culturing of U251 cells.

Transfection of Adherent Cells. Two million HEK293T cells were plated in a 10 cm^2 dish (Greiner Bio-one, Kremsmunster, Austria). The next day, cells were transfected with 100 ng of the different pcDEF3-US28 constructs and adjusted with empty pcDEF3 DNA to a total of 5 μg of DNA and 30 μg of 25 kDa linear polyethylenimine (Sigma-Aldrich) in 150 mM NaCl solution, resulting in a DNA/PEI ratio of 1:6. The DNA−PEI mixture was vortexed for 10 s and incubated for 15 min at room temperature (RT). Subsequently, the mixture was added dropwise to the adherent HEK293T cells.

Membrane Extract Preparation. To obtain membrane extracts, HEK293T-iUS28 or U251-iUS28 cells were induced with doxycycline as described above. Cells were washed with cold PBS and resuspended afterward in cold PBS. Cells were centrifuged at 1500*g* at 4 °C. Pellet was resuspended in cold PBS and again centrifuged at 1500*g* at 4 °C. The pellet was resuspended in membrane buffer (15 mM Tris-Cl, 0.3 mM EDTA, 2 mM MgCl2, pH 7.5) and disrupted by the Dounce Homogenizer Potter-Elvehjem at 1200 rpm.

Llama Immunization and Phage Display Library Construction. Two llamas were immunized using the pcDEF3 vector encoding for VHL/E US28. DNA was injected a total of eight times. Of these, four subcutaneous injections occurred in one stretch with 2-week intervals, which was followed by a lag-period of 5 weeks. These injections were followed up by two sets of boost injections, each consisting of two injections with a 2-week interval. One week after the final injections, blood was drawn and peripheral blood mononuclear cells were collected from both llamas, and total RNA was isolated. cDNA was obtained by reverse transcription-PCR using the SuperScriptTM^{IV} First-Strand Synthesis System (Invitrogen, Carlsbad, California, USA). Genes, encoding for the variable domains of the heavy-chain only antibodies, of both llamas were amplified using PCR and cloned into the pVUN014 phagemid vector and transformed into electro-competent *E. coli* TG1 (Lucigen), to make two libraries. Library sizes were estimated by means of a serial dilution of transformants. Different clones were picked and colony PCR

DOI: 10.1021/acs.molpharmaceut.9b00360
Mol. Pharmaceutics 2019, 16, 3145−3156

was performed using DreamTaq polymerase (Thermo Fisher Scientific) to determine the amount of clones containing a nanobody insert. The same PCR product was also cut with MvaI FastDigest (Thermo Fisher Scientific) to determine the diversity of clones in the library.

Phage Production. At the start of each selection round, 10 times the size of both nanobody libraries were pooled together (for round 1) or the rescues of the previous selection round (for rounds 2 and 3) were diluted in 2xTY broth containing 100 μg/mL ampicillin (Melford Biolabs ltd., Ipswich, UK) and 2% (w/v) glucose and grown until OD600 of 0.5. Cultures were infected with VCSM13 helper phage (Stratagene, San Diego, California, USA) at phage-bacteria ratio of 10:1−20:1. Cultures were grown 30 min without shaking followed by 30 min with shaking at 37 °C. Bacteria were centrifuged at 4500 rpm, and the pellet was resuspended in 2xTY broth containing 50 μg/mL kanamycin (Melford Biolabs Ltd.) and 100 μg/mL ampicillin. The culture was grown overnight at 28 °C to allow phage production. The next day, the culture was centrifuged at 4500 rpm, and supernatant was added to ice-cold 20% PEG6000/2.5 M NaCl (ratio 4:1) and incubated for 30 min on ice. The supernatant was centrifuged at 4000 rpm, and the phage pellet was resuspended in PBS. The phage solution was centrifuged, and the supernatant was again added to ice-cold 20% PEG6000/2.5 M NaCl and incubated for 10 min on ice. The supernatant was centrifuged again, and the phage pellet was resuspended in PBS.

Phage Display Selections. To obtain US28 specific binding nanobodies, three rounds of phage selections were performed using membrane extracts of the inducible US28 (VHL/E strain) HEK293T or U251 cell lines. Fifty micrograms of the membrane extracts were coated in a 96-well MicroWell MaxiSorp flat bottom plate (Sigma-Aldrich) overnight at 4 °C. Wells were washed three times with PBS and blocked with 2% (w/v) skimmed milk (Sigma-Aldrich) in PBS for 1 h at RT. Phages were diluted 1:10 (round 1) or 1:100 (rounds 2 and 3) in 0.2% (w/v) skimmed milk in PBS and added to the wells for 2 h at RT while shaking. If a counter-selection was performed during round 3, phages were first incubated with 250 μg of U251 membrane extracts for 1 h head-overhead (20 rpm) at RT. The mix was centrifuged at 4000 rpm, and the supernatant was added to the wells containing the membrane extracts of the induced US28 U251 cell line. After phage incubation, wells were washed 20 times with PBS with an incubation step of 10 min on a shaker each fifth washing step. Phages were eluted with 10 mg/mL Trypsin (Sigma-Aldrich) for 30 min at RT, and the eluate was mixed with 4 mg/mL 4-benzenesulfonyl fluoride hydrochloride (Sigma-Aldrich). Eluted phages were rescued by infecting TG1 cells (OD600 of 0.5) and grown overnight at 37 °C. Rescued phages were used for subsequent rounds of phage display. After 2 and 3 rounds of selections, bacteria were plated, and single colonies were grown in a 96-well plate containing 2xTY broth and 100 μg/mL ampicillin.

Phage Enzyme-Linked Immunosorbent Assay. Single colonies, picked after the second or third round of selections, were grown in 2xTY broth and 100 μg/mL ampicillin at 37 °C. When cultures were grown until OD600 of 0.5, the bacteria were infected with VCSM13 helper phage (end concentration 3.75×10^{13} pfu/mL). Cultures were grown 30 min without shaking followed by 30 min with shaking at 37 °C. 2xTY broth and 100 μg/mL ampicillin and kanamycin were added to obtain a final concentration of 50 μg/mL kanamycin. Cultures were grown overnight at 28 °C. Twenty-five micrograms of the membrane extracts with or without US28 were coated in a 96-well MicroWell MaxiSorp flat bottom plate overnight at 4 °C. The next day, wells were washed three times with PBS and blocked with 3% (w/v) skimmed milk in PBS for 1 h at RT. Phage cultures were centrifuged at 4000 rpm, and supernatant was added to 3% (w/v) skimmed milk in a 1:1 ratio and incubated for 1 h at RT on a shaker. Blocked phage solution was added to the MaxiSorp flat bottom plate containing membrane extracts with and without US28. Phages were incubated for 2 h at RT on a shaker. Wells were washed five times with PBS. Mouse-anti-$M13^{HRP}$ (GE-Healthcare, Chicago, Illinois, USA) was diluted 1:5000 in 3% (w/v) skimmed milk in PBS and incubated for 1 h at RT while shaking. The plates were washed again five times with PBS. *O*-Phenylenediamine (OPD) solution (2 mM OPD; Sigma-Aldrich, 35 mM citric acid, 66 mM Na_2HPO_4, 0.015% H_2O_2, pH 5.6) was added to the wells, and the reaction was stopped with 1 M H_2SO_4. Optical density was measured at 490 nm with a PowerWave plate reader (BioTek, Winooski, Vermont, USA), and the ratio of binding to the membrane extracts with and without US28 was determined.

Nanobody Production. Nanobody gene fragments were recloned in frame with a myc-His6 tag in the pET28a production vector and BL21 + *E. coli* were transformed by means of heat shock. Nanobodies were produced as described previously.[25] Purity of the nanobodies was verified by sodium dodecyl sulfate-polyacrylamide gel electrophoresis (SDS-PAGE) under reducing conditions (Bio-Rad, Hercules, California, USA).

ELISA Binding Assay. HEK293T or U251membrane extracts (20−50 μg) with or without US28 were coated in a 96-well MicroWell MaxiSorp flat bottom plate overnight at 4 °C. The next day, wells were washed three times with PBS and blocked with 2% (w/v) skimmed milk in PBS for 1 h at RT. Nanobodies were diluted in 2% (w/v) skimmed milk and incubated for 1 h at RT on a shaker. During the competition binding ELISA, 20 nM VUN100 was coincubated with previously described 100 nM untagged trivalent US28 nanobody or untagged trivalent irrelevant nanobody.[27] Nanobodies were detected with mouse-anti-Myc antibody (1:1000, Clone 9B11, Cell Signaling Technology, Leiden, The Netherlands) and horseradish peroxidase (HRP)-conjugated goat-antimouse antibody (1:1000, Bio-Rad). US28 expression was determined by means of rabbit-anti US28 antibody (Covance, Denver, USA, 1:2000, described previously[41]) and goat-antirabbit HRP-conjugated antibody (1:1000, Bio-Rad). All antibodies were diluted in 2% (w/v) skimmed milk and incubated for 1 h on a shaker at RT. Between each incubation step, wells were washed three times with PBS. After the last incubation steps, wells were washed three times with PBS and OPD was added to the wells, and the reaction was stopped with 1 M H_2SO_4. Optical density was measured at 490 nm with a PowerWave plate reader (BioTek). Data was analyzed using GraphPad Prism version 7.0 (GraphPad Software, Inc., La Jolla, CA, USA).

Competition Binding. Membrane extracts of HEK293T and HEK293T overexpressing US28 were used during competition binding studies. The experiments were performed as described previously.[27] Data was analyzed using GraphPad Prism version 7.0.

DOI: 10.1021/acs.molpharmaceut.9b00360
Mol. Pharmaceutics 2019, 16, 3145−3156

Phospholipase C Activation Assay. The activation of phospholipase C was assessed as described previously, and data was analyzed using GraphPad Prism version 7.0.[41]

Immunofluorescence Microscopy. Transiently transfected HEK293T or (US28-overexpressing) U251 cells were seeded in poly-L-lysine (Sigma-Aldrich) coated 96-well plates and were grown at 37 °C and 5% CO_2. Cells were prepared for immunofluorescence microscopy as described previously.[25] Briefly, cells were fixed with 4% paraformaldehyde (Sigma-Aldrich) for 10 min at RT and subsequently permeabilized with 0.5% NP-40 (Sigma-Aldrich) for 30 min at RT. Nanobodies were incubated for 1 h at RT and detected using Mouse-anti-Myc antibody (1:1000, 9B11 clone, Cell Signaling). US28 was visualized with the rabbit-anti-US28 antibody (1:1000, Covance[41]). Subsequently, cells were washed and incubated with Goat-anti-Rabbit Alexa Fluor 546 (1:1000 in 1% (v/v) FBS/PBS, Thermo Fisher Scientific) and Goat-anti-Mouse Alexa Fluor 488 (1:1000 in 1% (v/v) FBS/PBS, Thermo Fisher Scientific). When binding of VUN100 to CX3CR1 was assessed, receptor expression was detected using Rat-anti-HA antibody (1:1000 in 1% (v/v) FBS/PBS, Clone 3F10, Roche) or Rabbit-anti-HA antibody (1:1000 in 1% (v/v) FBS/PBS, H6908, Sigma-Aldrich) and Goat-anti-Rat Alexa Fluor 546 (1:1000 in 1% (v/v) FBS/PBS, Thermo Fisher Scientific) or Goat-anti-Rabbit Alexa Fluor 546 (1:1000 in 1% (v/v) FBS/PBS, Thermo Fisher Scientific). Cells were visualized with an Olympus FSX-100 microscope.

ELISA for US28 Expression. Transiently transfected HEK293T were seeded in poly-L-lysine (Sigma-Aldrich) coated 96-well plates and were grown at 37 °C and 5% CO_2. Cells were fixed with 4% paraformaldehyde (Sigma-Aldrich) for 10 min at RT. To assess total receptor expression, cells were subsequently permeabilized with 0.5% NP-40 (Sigma-Aldrich) for 30 min at RT. Cells were blocked for 30 min at RT in 1% (v/v) FBS/PBS. US28 constructs were detected with a rat-anti-HA antibody (1:1000 in 1% (v/v) FBS/PBS, Clone 3F10, Roche). Subsequently, wells were washed and incubated with HRP-conjugated goat-antirat antibody (1:1000 in 1% (v/v) FBS/PBS, Pierce). All antibodies were incubated for 1 h on a shaker at RT. Between each incubation step, wells were washed three times with PBS. After the last incubation steps, wells were washed three times with PBS and OPD was added to the wells, and the reaction was stopped with 1 M H_2SO_4. Optical density was measured at 490 nm with a PowerWave plate reader (BioTek). Data was analyzed using GraphPad Prism version 7.0 (GraphPad Software, Inc., La Jolla, CA, USA).

Immunohistochemistry. The experiments were performed as described previously.[27] US28 expression was detected using polyclonal rabbit-anti-US28 antibody (1:700, Covance), while nanobody binding was detected using mouse-anti-Myc antibody (1:500, 9B11 clone, Cell Signaling). MACH2 Universal HRP-Polymer detection was used as secondary antibody (Biocare Medical, Pacheco, California, USA).

Nanobody−Photosensitizer Conjugates. The nanobody gene was recloned into a pET28a vector to add a C-terminal cysteine (VUN100-Cys) for subsequent modification. Production was performed as described previously, and the nanobody was purified using chromatography (ÄKTAxpress) with 1 mL Histrap FF crude column (GE Healthcare) and 5 mL HiTrap Desalting column (GE Healthcare). The VUN100-Cys was incubated with 20 mM tris(2-carboxyethyl)phosphine (TCEP) at RT for 15 min. The buffer was replaced with 50 mM sodium phosphate containing 500 mM NaCl and 1 mM EDTA using Zeba spin desalting column (Thermo Fisher Scientific). The VUN100-Cys concentration was determined with the NanoDrop spectrophotometer (NanoDrop Technologies, Wilmington, Delaware, USA) at 280 nm. Immediately after buffer exchange, the VUN100-Cys (1 mg/mL) was mixed with 3 mol equiv of the photosensitizer IRDye700DX-maleimide and incubated overnight at 4 °C on a rotator. The next day, the free photosensitizer was removed by passing the solution through three consecutive Zeba spin desalting columns, which were pre-equilibrated with 2 M NaCl in PBS. The degree of conjugation and concentration of the protein was determined as described previously.[12] The purity and the integrity of the nanobody−photosensitizer conjugate was determined on SDS-PAGE gel. The gel was imaged on an Odyssey Infrared scanner at 700 nm (LI-COR Biosciences, Lincoln, Nebraska, USA).

LC−MS of Nanobody−Photosensitizer Conjugates. Intact nanobody−photosensitizer conjugates were analyzed with ultrahigh performance liquid chromatography mass-spectrometry (UHPLC-MS). The system consisted of a 1290 Infinity UHPLC-UV system (Agilent Technologies, Waldbronn, Germany) connected to an Agilent Technologies 6560 ion mobility quadrupole time-of-flight mass spectrometer with a jet stream electrospray ionization interface, operated in positive ion mode. Separation was achieved using an Acquity UPLC protein BEH C4 column (50 × 2.1 mm, 300 Å, 1.7 μm particles, Waters, Milford, Massachusetts, USA), which was maintained at 70 °C during analysis. A 1 μL sample volume was injected into the system, and analytes were separated using linear gradient elution with 0.1% formic acid (solvent A) and 0.1% formic acid/acetonitrile 5:95 (v/v) (solvent B), increasing from 20 to 40% B in 10 min at a flow rate of 0.30 mL/min. Detection was performed with UV at 280 nm and MS using a capillary voltage of 5.5 kV, a nozzle voltage of 2 kV, a nitrogen nebulizing pressure of 45 psi, a nitrogen sheath gas flow of 11 L/min at 400 °C, and a drying gas flow of 8 L/min at 350 °C. Data were acquired between m/z 300−3200 and processed using Agilent Technologies MassHunter software (version B.08.00).

Determination of the Expression of US28 Receptor. To determine the number of US28 expressing U251 cells upon induction with doxycycline for 48 h, US28 positive cells were seeded in a 96-well plate. Cells were fixed with 4% PFA for 10 min at RT and then incubated with 100 mM glycine for 10 min at RT, subsequently permeabilized with 0.5% Triton X-100 for 10 min at RT. The cells were blocked with 2% BSA for 30 min at RT. Cells were incubated with polyclonal rabbit anti-US28 primary antibody (1:1000 diluted in blocking buffer) for 1 h at RT. After multiple washing steps, Goat-anti-Rabbit Alexa 488 secondary antibody (1:1000 diluted in blocking buffer) and TO-PRO-3 (1 μM, Thermo Fisher Scientific) were added to the cells and incubated for 1 h at RT. The cells were imaged with an EVOS microscope and analyzed with ImageJ. The US28 expressing cells were detected by antibody staining, and the percentage was calculated related to the total cell number (detected with TO-PRO-3).

Cell Binding Assay with Nanobody−Photosensitizer. U251-iUS28 were induced for 48 h with doxycycline resulting in U251 cells overexpressing US28 (US28 positive) and the control (US28 negative) cells (if not induced) as described earlier.[45] US28 positive and US28 negative cells were seeded at

DOI: 10.1021/acs.molpharmaceut.9b00360
Mol. Pharmaceutics 2019, 16, 3145−3156

8000 cells per well in a 96-well plate (Nunc, Roskilde, Denmark). The next day, cells were washed once with binding medium (DMEM without phenol red, 25 mM HEPES, and 1% BSA, pH 7.4). Subsequently, different concentrations of nanobody−photosensitizer were added to the plate and incubated for 2 h at 4 °C. Unbound nanobody−photosensitizer conjugate was removed by washing three times with binding buffer. The amount of bound nanobody−photosensitizer was detected with Odyssey infrared scanner (Li-COR) at 700 nm. Data was analyzed using GraphPad Prism version 7.0.

In Vitro PDT. The US28 positive and negative U251 cells were washed with washing medium (DMEM medium without phenol red, 10% FBS, 1% penicillin/streptomycin). The cells were incubated with different concentrations of nanobody−photosensitizer for 1 h at 37 °C. Cells were washed two times with washing medium, and bound and/or internalized nanobody−photosensitizer was detected using the Odyssey infrared scanner at 700 nm. Next, cells were illuminated 33 min with 5 mW/cm^2 fluence rate for a total light dose of 10 J/cm^2 using a 690 nm diode laser through a 600 μM optic fiber (Modulight, Tampere, Finland). After overnight incubation of the cells at 37 °C, the viability of the cells was assessed by AlamarBlue reagent, as recommended by manufacturer (Bio-Rad). Cell viability was measured with a Fluostar Optima fluorescent plate reader (BMG Labtech GmbH, Ortenberg, Germany). Cells that were neither illuminated nor treated were used to determine 100% cell viability. The percentage of cell viability was calculated relative to the untreated cells, and data was analyzed using GraphPad Prism version 7.0.

Coculture Assay. The US28 positive and negative U251 cells were coseeded in a 96-well plate in various ratios. After 1 h of incubation with 50 nM of nanobody−photosensitizer, the cells were illuminated with total light dose of 10 J/cm^2. After overnight incubation of the cells at 37 °C, cells were incubated with propidium iodide (1 μg/mL, Invitrogen) and calcein AM (0.5 μg/mL, Invitrogen) for 10 min at 37 °C. The cells were imaged with an EVOS microscope and counted with ImageJ. The theoretical percentage of positive cells versus percentage of dead cells was plotted.

In Vitro PDT in 3D spheroids. The US28 positive and negative U251 cells were seeded in an ultralow attachment U bottom 96-well plate (Corning). Two days after seeding, 50 μL of the medium was removed from each well, and spheroids were incubated with different concentrations of nanobody−photosensitizer in washing medium for 1 h at 37 °C. After three times washing of the spheroids with the same medium, the plate was illuminated 33 min with 5 mW/cm^2 fluence rate for a total light dose of 10 J/cm^2 using a 690 nm diode laser through a 600 μM optic fiber (Modulight). After overnight incubation at 37 °C, the viability was assessed by CellTiter-Glo 3D reagent as recommended by the manufacturer (Promega, Madison, Wisconsin, USA). The percentage of cell viability was calculated relative to the untreated cells. Data was analyzed using GraphPad Prism version 7.0.

Statistical Analysis. Statistical significance was determined by unpaired Student's t test. Significant values were set as indicated in figure legends.

RESULTS

Selection and Characterization of a New US28 Nanobody. In this study, we set out to develop a novel US28-targeting nanobody−photosensitizer conjugate to eradicate US28-expressing tumor cells via targeted PDT. This approach requires a nanobody with high affinity and specificity for US28. Because of the relatively poor binding affinity of the monovalent US28 nanobody published earlier,[27] we developed new nanobodies with higher affinity for US28. Phage libraries with nanobody genes were constructed after immunization of llamas with US28 DNA. Upon panning selections, 330 clones were screened for selective binding to US28 by means of a phage ELISA. Of these 330 screened clones, 85 were positive for specific binding to US28 and could be divided in 7 different groups based on their CDR3 regions. Interestingly, one of the US28-binding nanobody clones contained a similar CDR3 as the previously published US28 nanobody.[27] This new nanobody was named VUN100 and further characterized. Importantly, VUN100 bound US28 of membranes obtained from US28-overexpressing cells with a binding affinity of 2 ± 1 nM, which is approximately 170-fold higher than the previously reported US28 nanobody (US28 Nb) (340 ± 80 nM) (Figure 1A). To ensure selectivity, binding of VUN100 to

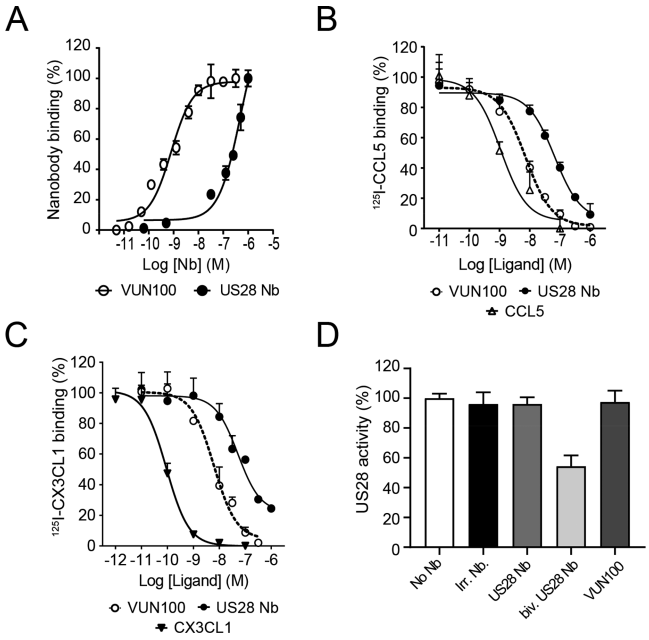

Figure 1. VUN100 binds the HCMV-encoded US28 with high affinity. (A) Binding of the nanobodies VUN100 and US28 Nb to US28-expressing membranes, as determined by ELISA. (B,C) Displacement of ^{125}I-CCL5 (B) and ^{125}I-CX3CL1 (C) from US28-expressing membranes by unlabeled ligand or the nanobodies VUN100 and US28 Nb. (D) Effect of nanobodies on the US28-mediated phospholipase C activation. No Nb, No nanobody; Irr. Nb, Irrelevant nanobody; biv. US28 Nb, bivalent US28 nanobody.

US28 was compared to the binding of an irrelevant Nb (binding to the azodye reactive red 6, RR6) (Figure S1A) and binding of VUN100 to the chemokine receptor CX3CR1, with which US28 shares the highest homology, were assessed (Figure S1B). No binding of the irrelevant nanobody to US28 was seen, and VUN100 did not show any binding to CX3CR1. VUN100 displaced ^{125}I-CCL5 with a K_i value of 6 ± 1 nM, compared to 142 ± 49 nM for the previous US28 nanobody (Figure 1B,C and Table 1). Similarly, VUN100 displaced ^{125}I-CX3CL1 with a potency of 6 ± 1 nM, compared to 100 ± 58 nM for the previous US28 nanobody. This improvement in potency of approximately 20-fold was in line with the increased

DOI: 10.1021/acs.molpharmaceut.9b00360
Mol. Pharmaceutics 2019, 16, 3145−3156

Table 1. Pharmacological Characteristics of Nanobodies Targeting US28

nanobody	k_D (nM, ±SD)	K_i CCL5 (nM, ±SD)	K_i CX3CL1 (nM, ±SD)
US28 Nb	340 ± 80	142 ± 49	100 ± 58
VUN100	2 ± 1	6 ± 1	6 ± 1

binding affinity of VUN100 for US28. Despite this increase in affinity, VUN100 did not affect the US28 constitutive activity (Figure 1D). As the previous monovalent US28 Nb, VUN100 did not show any inverse agonistic properties, while the previously reported bivalent US28 Nb was able to partially inhibit US28 signaling.[27] In conclusion, new immunizations and selections yielded a new US28 targeting nanobody with a superior binding affinity and potency in chemokine displacement.

VUN100 Binds to the N-terminus and ECL3 of US28. In order to determine which domains of US28 are essential for binding of VUN100, binding was assessed on US28 mutants in immunofluorescence microscopy. While clear binding of VUN100 to US28 wild type (WT) was observed, binding of VUN100 was lost when the first 22 amino acids of the N-terminus of US28 were removed (Figure 2A). This was also observed for the previously published US28 nanobody.[27] This observation, together with the similarity in CDR3 regions, suggest that both nanobodies bind to a similar epitope of US28. The US28 Nb was able to displace binding of VUN100 to US28, further corroborating that they bind a similar region of US28 (Figure S2A). To study the binding epitope of VUN100 in more detail, binding of VUN100 was assessed on US28 mutants with point mutations in the N-terminus. Mutations of the amino acids to alanines at positions 11 to 15 did not have any effect on the binding of VUN100 (Figure S2B). Interestingly, mutation of the tyrosine at position 16 to a phenylalanine (US28 Y16F) resulted in impaired binding of VUN100. This suggests that this tyrosine is important for binding of VUN100 to US28. Since nanobodies are known to bind discontinuous epitopes, US28 extracellular loop (ECL) mutants were constructed. Due to the homology of CCR5 with US28 and CCL5 binding to both receptors, chimeric receptors were constructed in which the ECLs of US28 were replaced with the corresponding ECLs of CCR5. To ensure proper folding and expression of the chimeric receptors, the (surface) expression was confirmed by ELISA (Figure 2B). Next, binding of VUN100 to these chimeras was assessed (Figure 2C). The substitution of the ECL1 (US28 ECL1-CCR5) and ECL2 (US28 ECL2-CCR5) did not influence the binding of VUN100. However, the substitution of the ECL3 (US28 ECL3-CCR5) resulted in the loss of binding of VUN100. These results were further confirmed by determining the binding affinity on membrane extracts expressing the different US28 mutants (Figure 2D). These data indicate that VUN100 binds a discontinuous epitope on the extracellular side of US28 that involves tyrosine 16 in the N-terminus and ECL3.

Also in US28-expressing glioblastoma cells, VUN100 was able to bind US28 (Figure 3A). US28 has been detected in multiple cancers of which US28 expression in glioblastoma is the most widely studied. Therefore, detection of US28 in glioblastoma sections of HCMV-infected glioblastoma patients by these nanobodies was assessed. A comparable US28 expression pattern in glioblastoma was detected by both the

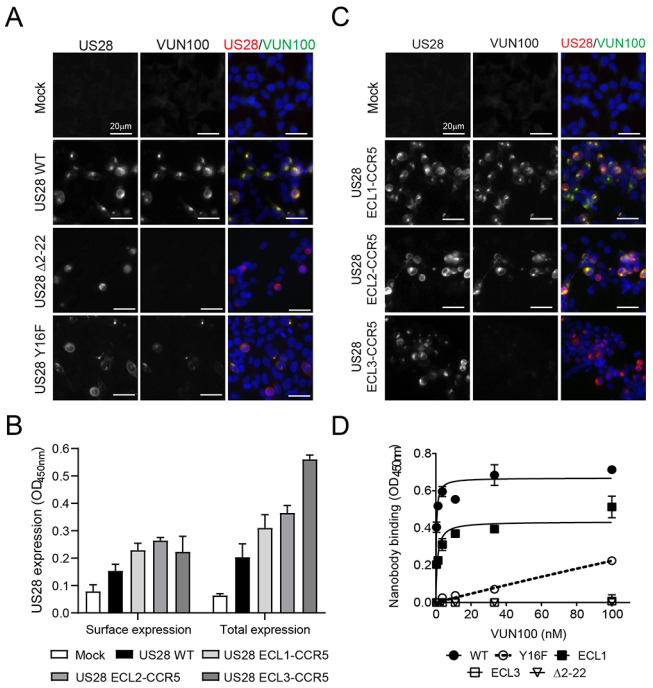

Figure 2. VUN100 binds to the N-terminus and ECL3 loop of US28. (A) Immunofluorescence microscopy of the binding of VUN100 to Mock, US28 wild-type (US28 WT), N-terminus truncated US28 (US28-Δ2-22), and US28 with mutation of the tyrosine at position 16 to a phenylalanine (US28 Y16F). US28 was detected using an anti-US28 antibody (US28). VUN100 binding was detected using the Myc-tag and an anti-Myc antibody (VUN100). (B) Detection of surface and total expression of HA-tagged US28 wildtype (US28 WT) and HA-tagged US28 chimeras with the CL1−3 loop being substituted by the corresponding loops of CCR5. Receptor expression was detected by the N-terminal HA-tag. (C) Immunofluorescence microscopy of the binding of VUN100 to Mock transfected or US28 chimeras with the ECL1−3 loop being substituted by the corresponding loops of CCR5. US28 was detected using an anti-US28 antibody (US28). VUN100 binding was detected using the Myc-tag and an anti-Myc antibody (VUN100). (D) Binding ELISA of different concentrations of VUN100 to membranes of HEK293T cells transfected with wild-type US28 (WT), US28 Y16F (Y16F), US28 ECL1-CCR5 chimera (ECL1), US28 ECL3-CCR5 chimera (ECL3), and US28-Δ2-22 (Δ2-22).

polyclonal anti-US28 antibody directed against the C-terminus of US28, and the two US28 targeting nanobodies (Figure 3B).

Taken together, the newly selected anti-US28 nanobody VUN100 shows high affinity for the extracellular domains of US28 and binds to US28 in HCMV-positive glioblastoma tissues. This makes VUN100 therefore a suitable targeting moiety for US28-targeted therapies.

Site-Directed Conjugation of IRDye700DX to VUN100. To facilitate the specific killing of US28-expressing tumor cells by PDT, the water-soluble photosensitizer IRDye700DX was conjugated to VUN100. Previously, this conjugation was done for other nanobodies through random labeling of lysine residues using NHS-coupling.[12,13] However, conjugation to lysines in VUN100 led to a loss of binding capacity to US28 (Figure S3A). This is likely due to presence of lysines in and near the CDR regions of VUN100. To resolve this, a VUN100 variant with an additional cysteine in a C-terminal tag (VUN100-Cys) was produced. The addition of this cysteine did not have any effect on the affinity of the

DOI: 10.1021/acs.molpharmaceut.9b00360
Mol. Pharmaceutics 2019, 16, 3145−3156

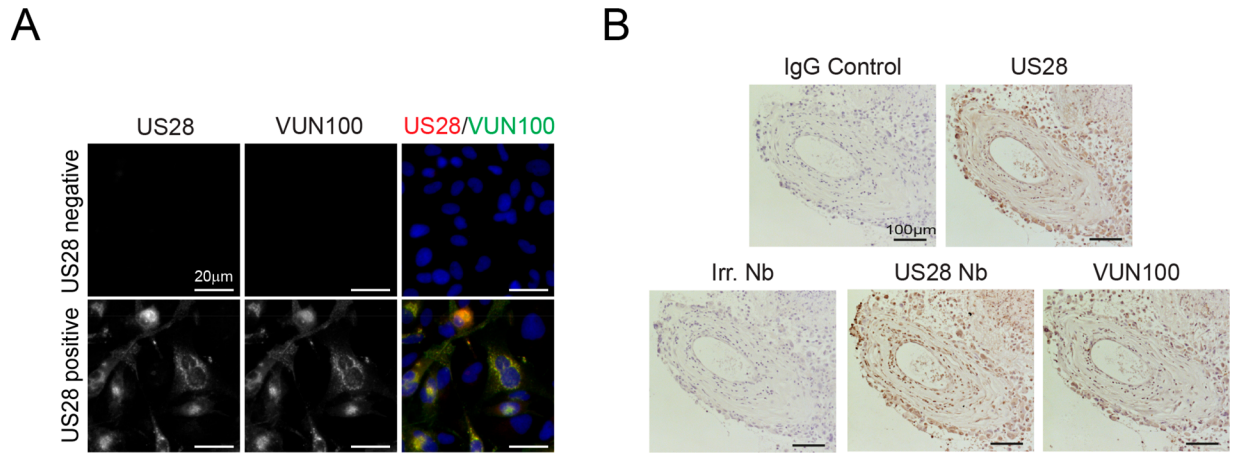

Figure 3. VUN100 binds US28 in glioblastoma cells and glioblastoma patient material. (A) Immunofluorescence microscopy of the binding of VUN100 to glioblastoma cells (US28 negative) and glioblastoma cells expressing US28 (US28 positive). US28 was detected using an anti-US28 antibody (US28). VUN100 binding was detected using the Myc-tag and an anti-Myc antibody (VUN100). (B) Detection of US28 in parallel sections of glioblastoma patient material. Nuclei were stained using Hoechst staining (blue). US28 was detected using an anti-US28 antibody (US28). Nanobodies were detected via their Myc-tag (brown). An IgG isotype control and irrelevant nanobody (Irr. Nb) were used as controls.

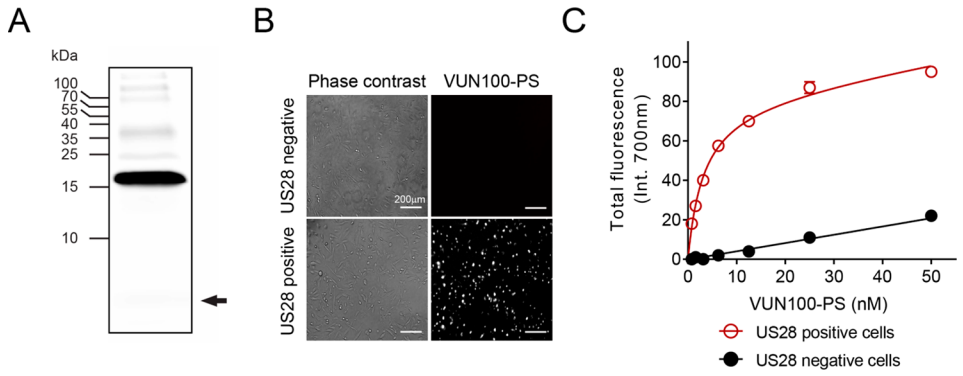

Figure 4. Binding of VUN100-PS conjugates to US28. (A) SDS-PAGE of the VUN100-IRDye 700DX conjugate (VUN100-PS). A small quantity of free photosensitizer is observed at the gel front (arrow). (B) Binding of VUN100-PS to US28 negative (US28 negative) and US28 positive U251 glioblastoma cells (US28 positive). U251-iUS28 were induced for 48 h with doxycycline resulting in US28 positive glioblastoma cells US28 negative glioblastoma cells (if not induced). VUN100-PS was visualized with a widefield fluorescent microscope. (C) Binding of different concentrations of VUN100-PS to US28 negative and positive cells on ice. Fluorescence of VUN100-PS bound to cells was detected using an Odyssey infrared scanner at 700 nm.

nanobody to US28 (Figure S3B) but enabled site-directional conjugation of the photosensitizer to VUN100 by maleimide-coupling. Site-directed conjugation and purification resulted in a VUN100-PS conjugate of ~15 kDa with a degree of conjugation (DOC) of 0.7 molecules of photosensitizer per nanobody and less than 2% of free photosensitizer (Figure 4A). Besides the VUN100-PS conjugate, small amounts of other fluorescent products were detected on the SDS-PAGE, which are likely impurities conjugated to the photosensitizer. VUN100-PS was also analyzed by UHPLC−MS, providing separation of conjugated and unconjugated nanobody and identification by their deconvoluted mass. The mass difference between unconjugated (15.2 kDa) and conjugated nanobody (17.1 kDa) corresponded well to the mass of the photosensitizer (1.9 kDa), confirming the conjugation of one nanobody with a single photosensitizer molecule (Figure S4). The percentage area of conjugated nanobody in the chromatograms, with respect to total nanobody area, was 71.3% with UV and 71.8% with MS detection, which corresponded well with the obtained DOC of 0.7. Directional conjugation of the photosensitizer to the nanobody did not affect its binding capacity, as binding of VUN100-PS to US28 positive cells and not to negative cells was observed by immunofluorescence microscopy (Figure 4B). In addition, VUN100-PS bound US28 positive cells with a binding affinity of 3.1 ± 0.1 nM, while no specific binding was seen on US28 negative cells (Figure 4C). These results indicate that the site-directed conjugation of the photosensitizer to VUN100 was successful and did not change the binding properties of VUN100 to US28.

VUN100-Targeted PDT Selectively Kills US28 Positive Cells. Next, the ability of the VUN100-PS conjugate to kill US28 positive cells was assessed. First, the percentage of US28 positive cells upon induction with doxycycline was quantified. Immunofluorescence staining showed that 89 ± 3% of the cell population was US28 positive after 48 h of induction (Figure 5A). Next, the effect of VUN100-PS on US28 positive and negative cells was assessed. During a pulse of 1 h at 37 °C VUN100-PS associated specifically with the US28 positive cells (Figure 5B). One day after the activation of the photosensitizer by a light dose of 10 J/cm^2, cell viability was determined. US28-targeted PDT resulted in up to 90% reduction in cell viability of US28 positive cells with an EC_{50} value of 1.1 ± 0.2 nM (Figure 5C). These percentages of cytotoxicity correlated

DOI: 10.1021/acs.molpharmaceut.9b00360
Mol. Pharmaceutics 2019, 16, 3145−3156

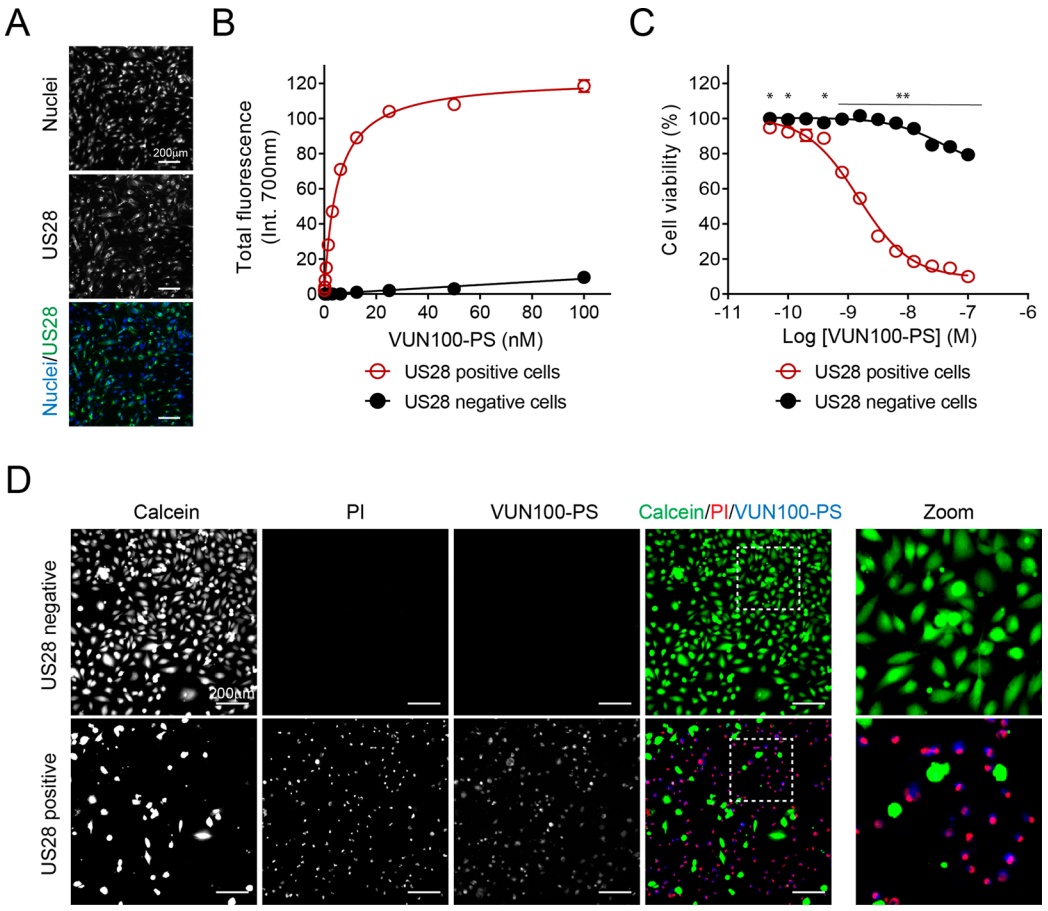

Figure 5. VUN100-PS selectively kills US28-expressing cells upon illumination. (A) Staining of US28 after 48 h of doxycycline-induction of US28-expressing glioblastoma cells. US28 was visualized using anti-US28 antibody and the percentage of US28-positive cells was determined using ImageJ. (B) Detection of different concentrations of bound and internalized VUN100 to US28 positive and negative cells. Binding was determined using Odyssey infrared scanner at 700 nm. (C) Determination of cell viability after incubation with different concentrations of VUN100-PS and illumination 10 J/cm^2 light dose. Cell viability was determined using Alamar blue reagent (*, $p < 0.05$; **, $p < 0.01$, t test). (D) Staining of dead cells with propidium iodide (PI) and living cells (calcein) 24 h after nanobody-targeted PDT using 50 nM VUN100-PS, performed as described above.

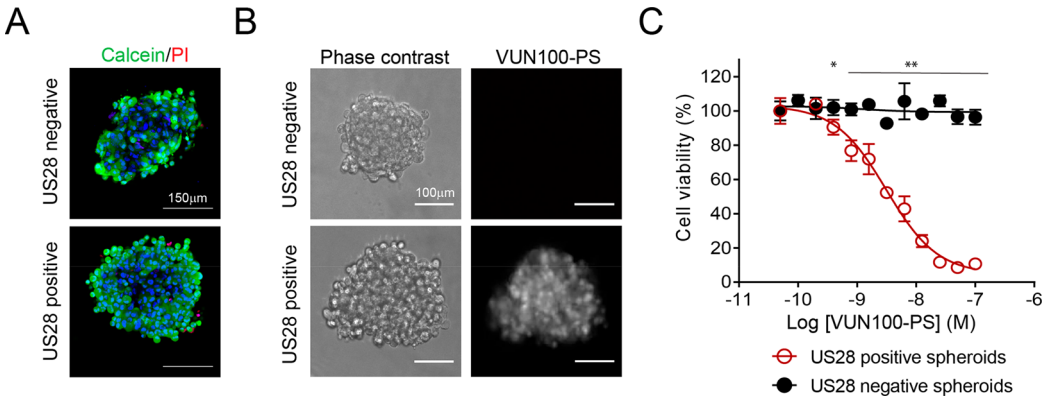

Figure 6. VUN100-PS selectively binds to US28-expressing spheroids and induces cell toxicity upon illumination. (A) Staining of dead cells with propidium iodide (PI) and living cells (calcein) of US28 negative spheroids (US28 negative) and US28 positive spheroids (US28 positive). (B) Incubation of VUN100-PS with US28 negative and positive spheroids. Spheroids and VUN100-PS were visualized with an EVOS microscope. (C) Determination of cell viability after incubation with different concentrations of VUN100-PS and illumination with a 10 J/cm^2 light dose. Cell viability was determined using CellTiter-Glo 3D reagent (*, $p < 0.05$; **, $p < 0.01$, t test).

well with the percentage of US28-expressing cells upon induction by doxycycline as shown in Figure 5A. The selective cell killing by VUN100-targeted PDT was confirmed by staining with propidium iodide (dead cells) and calcein (living cells). Staining of propidium iodide in cells correlated well with the VUN100-PS binding, indicating that only those cells expressing US28 and able to bind VUN100-PS died (Figure 5D). The few viable cells that remained did not show

DOI: 10.1021/acs.molpharmaceut.9b00360
Mol. Pharmaceutics 2019, 16, 3145−3156

association of VUN100-PS or propidium iodide staining. To further determine the selectivity and local effect of nanobody-targeted PDT, coculture experiments with different ratios of US28 positive and US28 negative cells were performed. Even in the case of decreasing number of US28 positive cells, a clear decrease in number of killed cells is observed, suggesting VUN100-PS targeted PDT killed the US28 positive cells and did not affect the US28 negative cells (Figure S5). This confirms that, in close proximity of US28 negative and positive cells, the short activity range of the activated photosensitizer allows the selective killing of targeted cells while leaving the negative cells unaffected.

VUN100-Targeted PDT Efficiently Induces Cell Toxicity in US28 Expressing 3D Spheroids. To test the efficacy of VUN100-targeted PDT in a more relevant setting, its effect was tested on 3D spheroid cultures of US28 expressing and US28 negative glioblastoma cells. After 2 days of seeding, both types of spheroids were viable (Figure 6A). After 1 h of incubation with VUN100-PS, association of VUN100-PS to the US28 positive spheroids was observed, while no fluorescence of VUN100-PS was observed for the US28 negative spheroids (Figure 6B). Next, spheroids were illuminated with near-infrared light, and cell viability was assessed. In line with the results from the 2D culture experiments, VUN100-PS selectively induced cell death in up to 90% of the cells in the US28 positive spheroids with an EC_{50} value of 4.1 ± 1.6 nM, while no cell death was observed in the US28 negative spheroids (Figure 6C).

DISCUSSION

Multiple GPCRs, including chemokine receptors, are overexpressed in tumors including melanomas, breast, lung, colorectal, and head and neck cancer making them interesting targets for targeted therapies.[26,46−50] In this study, we set out to investigate the potential of GPCRs as targets for nanobody-targeted PDT by using the HCMV-encoded chemokine receptor US28 as a proof of concept. We developed a new US28 targeting nanobody (VUN100) with a superior binding affinity for US28, compared to our previously reported US28 nanobody.[27] Interestingly, different llamas, immunization procedures, and distinct selection strategies resulted in the identification of a nanobody with high sequence similarity in the CDR3 region. Moreover, VUN100 bound the same epitope on US28, as the previously described US28 nanobody, although with a higher affinity. Because of the high CDR3 homology between these two different nanobodies, the increased affinity can be ascribed to differences in the frameworks and other CDR regions. This confirms the general notion that the CDR3 region plays a predominant role in determining the binding epitope of nanobodies, while affinity variations are more likely the consequence of variations in CDR and framework sequences.[51−53] The epitope of VUN100 involved both the N-terminus and ECL3 loop of US28. More specifically, although more residues in the N-terminus might be involved, the tyrosine at position 16 is important for binding of VUN100. In a previous study, this residue (and more specifically the sulfonyl group) was also found to be important for ligand binding, which correlates well with the observation that VUN100 displaces the known US28 ligands CCL5 and CX3CL1.[54] Although VUN100 could displace multiple types of chemokine ligands from US28, we observed no nonspecific binding of VUN100 to CX3CR1, which is the chemokine receptor that shares the highest homology with US28, indicating the specificity of VUN100 for US28.

Our experiments show that nanobody-targeted PDT induced cell death of up to 90% of the US28 expressing cells. This percentage correlates with the percentage of cells with detectable US28 expression. However, it is currently unclear whether the cells that escaped PDT-mediated cell death are truly US28 negative or express the receptor at low levels. Using a stable cell line, it is likely that these presumably negative cells do express low levels of US28, though undetectable. The efficacy of the treatment could be enhanced further by increasing the amount of photosensitizer delivered to these cells. In contrast to a maximal degree of conjugation of 1 by directional conjugation, higher conjugation efficacies could potentially be achieved by random conjugation of photosensitizer to multiple lysines. However, conjugation to multiple lysines cannot be controlled easily and can also significantly harm the integrity of the nanobody (as was here observed for VUN100). Another way of increasing the delivery of photosensitizer is by intracellular delivery and residualization of the conjugate, such that the photosensitizer will accumulate in the cell. Depending on the chemical properties and size of fluorescent dyes, these molecules can residualize inside cells upon uptake. Using the endocytic machinery in cells, extended pulses with nanobody−photosensitizer conjugates could result in intracellular accumulation of photosensitizer, which would favor PDT efficacy. Near-infrared dye IRDye800CW and the photosensitizer IRDye700DX are both known to residualize inside cells.[12,55] Previously, we have shown the additional PDT effect with an internalizing anti-EGFR nanobody−photosensitizer conjugate.[12] US28 is known to be constitutively internalized.[56] Potentially, this would allow repetitive uptake and accumulation of photosensitizer-conjugated nanobodies in US28-expressing cells, thereby enhancing PDT efficacy.

Antibodies have already shown to be good targeting moieties for targeted PDT.[6,7] However, their relatively large size, together with the binding site barrier hampers their tissue distribution.[57] Previous studies have already shown a faster and more homogeneous distribution of nanobodies compared to antibodies.[13,58,59] Recently, the penetration of EGFR-targeted nanobodies and the anti-EGFR monoclonal antibody cetuximab were assessed in 3D spheroids.[60] A clear delay in accumulation in the spheroid was seen for the monoclonal antibody compared to the nanobodies. In this study, selective killing of US28-positive glioblastoma cells was observed both in 2D and 3D cultures. Furthermore, no significant difference in efficacy was observed between PDT in 2D or 3D cultures. These results further substantiate the potential use of nanobody−photosensitizer conjugates for GPCR-targeted PDT.

Although the blood−brain barrier is considered to be leaky in glioblastoma patients, different strategies have been described to enhance the crossing of nanobodies through the blood−brain barrier, including the modification of the isoelectric point of nanobodies.[61−65] Currently, conventional (untargeted) PDT is approved for intraoperative PDT of malignant brain tumors in Japan, making the application of nanobody-targeted PDT in the brain therefore conceivable.[66,67]

In this study, US28 was used as an example for GPCR-targeted PDT. Importantly, US28 expression is detected in various tumors, whereas it is only detected in a small

DOI: 10.1021/acs.molpharmaceut.9b00360
Mol. Pharmaceutics 2019, 16, 3145−3156

percentage of latently infected myeloid cells in healthy individuals, making this receptor a very interesting (nonhuman) target for targeted therapies.[32−38,68] In addition, an US28-targeting fusion toxin protein was able to kill latently infected myeloid cells, indicating the potential of US28-targeted therapies to eradicate HCMV-infected cells.[69] Although we are the first to describe GPCRs as targets for nanobody-targeted PDT, GPCR-targeted PDT has been reported previously for the type 2 cannabinoid receptor (CB_2R).[70] A CB_2R-targeting small molecule (mbc94) was conjugated to the photosensitizer IRDye700DX and killed around 80% of the CB_2R-overexpressing cells. However, this required micromolar concentrations of the conjugate, overnight incubation periods with conjugates, and illumination with higher power density (30 mW/cm^2 and a total dose of 36 J/cm^2). With VUN100-PS, we were able to selectively induce cell toxicity in US28-positive glioblastoma cells after 1 h of incubation with conjugates, a power density of 5 mW/cm^2, and a total dose of 10 J/cm^2, resulting in nanomolar potency values. For these reasons, GPCR-targeting nanobodies have good potential for *in vivo* PDT.

To conclude, by using a novel US28-targeting nanobody−photosensitizer conjugate we selectively killed US28-expressing glioblastoma cells both in 2D and 3D cultures. This study shows the potential of GPCRs as targets for nanobody-directed PDT to treat proliferative diseases. In addition, US28-targeting nanobody−photosensitizer conjugates hold potential in treatment of HCMV-associated malignancies.

■ ASSOCIATED CONTENT

Supporting Information

The Supporting Information is available free of charge on the ACS Publications website at DOI: 10.1021/acs.molpharmaceut.9b00360.

Selectivity binding assays, epitope binding, nanobody binding, ultraperformance liquid chromatography−mass spectrometry, photodynamic therapy treatment (PDF)

■ AUTHOR INFORMATION

Corresponding Author

*E-mail: mj.smit@vu.nl. Tel: +31205987572.

ORCID

Martine J. Smit: 0000-0003-2713-0238

Sabrina Oliveira: 0000-0002-6011-2122

Author Contributions

[#]These authors contributed equally. [▽]These authors contributed equally.

Notes

The authors declare the following competing financial interest(s): R.H. is affiliated with QVQ Holding BV, a company offering VHH services and VHH-based imaging molecules. All other authors declare no conflict of interest.

■ ACKNOWLEDGMENTS

This work was supported by The Netherlands Organization for Scientific Research (NWO: Vici grant 016.140.657) and the European Research Council (ERC) under the European Union's Horizon 2020 research and innovation program (grant agreement No 677582).

■ ABBREVIATIONS

PDT, photodynamic therapy; GPCR, G protein-coupled receptor; EGFR, epidermal growth factor receptor; HCMV, human cytomegalovirus; ECL, extracellular loop; DOC, degree of conjugation; PI, propidium iodide

■ REFERENCES

(1) Agostinis, P.; Berg, K.; Cengel, K. A.; Foster, T. H.; Girotti, A. W.; Gollnick, S. O.; Hahn, S. M.; Hamblin, M. R.; Juzeniene, A.; Kessel, D.; Korbelik, M.; Moan, J.; Mroz, P.; Nowis, D.; Piette, J.; Wilson, B. C.; Golab, J. Photodynamic therapy of cancer: an update. *Ca-Cancer J. Clin.* **2011**, *61* (4), 250−81.

(2) Kwiatkowski, S.; Knap, B.; Przystupski, D.; Saczko, J.; Kedzierska, E.; Knap-Czop, K.; Kotlinska, J.; Michel, O.; Kotowski, K.; Kulbacka, J. Photodynamic therapy - mechanisms, photosensitizers and combinations. *Biomed. Pharmacother.* **2018**, *106*, 1098−1107.

(3) Calixto, G. M.; Bernegossi, J.; de Freitas, L. M.; Fontana, C. R.; Chorilli, M. Nanotechnology-Based Drug Delivery Systems for Photodynamic Therapy of Cancer: A Review. *Molecules* **2016**, *21* (3), 342.

(4) Martinez De Pinillos Bayona, A.; Mroz, P.; Thunshelle, C.; Hamblin, M. R. Design features for optimization of tetrapyrrole macrocycles as antimicrobial and anticancer photosensitizers. *Chem. Biol. Drug Des.* **2017**, *89* (2), 192−206.

(5) Gomer, C. J. Preclinical examination of first and second generation photosensitizers used in photodynamic therapy. *Photochem. Photobiol.* **1991**, *54* (6), 1093−107.

(6) van Dongen, G. A.; Visser, G. W.; Vrouenraets, M. B. Photosensitizer-antibody conjugates for detection and therapy of cancer. *Adv. Drug Delivery Rev.* **2004**, *56* (1), 31−52.

(7) Mitsunaga, M.; Ogawa, M.; Kosaka, N.; Rosenblum, L. T.; Choyke, P. L.; Kobayashi, H. Cancer cell-selective in vivo near infrared photoimmunotherapy targeting specific membrane molecules. *Nat. Med.* **2011**, *17* (12), 1685−91.

(8) van Straten, D.; Mashayekhi, V.; de Bruijn, H. S.; Oliveira, S.; Robinson, D. J. Oncologic Photodynamic Therapy: Basic Principles, Current Clinical Status and Future Directions. *Cancers (Basel)* **2017**, *9* (12), 19.

(9) Beckman, R. A.; Weiner, L. M.; Davis, H. M. Antibody constructs in cancer therapy: protein engineering strategies to improve exposure in solid tumors. *Cancer* **2007**, *109* (2), 170−9.

(10) Thurber, G. M.; Zajic, S. C.; Wittrup, K. D. Theoretic criteria for antibody penetration into solid tumors and micrometastases. *J. Nucl. Med.* **2007**, *48* (6), 995−9.

(11) Watanabe, R.; Hanaoka, H.; Sato, K.; Nagaya, T.; Harada, T.; Mitsunaga, M.; Kim, I.; Paik, C. H.; Wu, A. M.; Choyke, P. L.; Kobayashi, H. Photoimmunotherapy targeting prostate-specific membrane antigen: are antibody fragments as effective as antibodies? *J. Nucl. Med.* **2015**, *56* (1), 140−4.

(12) Heukers, R.; van Bergen en Henegouwen, P. M.; Oliveira, S. Nanobody-photosensitizer conjugates for targeted photodynamic therapy. *Nanomedicine* **2014**, *10* (7), 1441−51.

(13) van Driel, P.; Boonstra, M. C.; Slooter, M. D.; Heukers, R.; Stammes, M. A.; Snoeks, T. J. A.; de Bruijn, H. S.; van Diest, P. J.; Vahrmeijer, A. L.; van Bergen En Henegouwen, P. M. P.; van de Velde, C. J. H.; Lowik, C.; Robinson, D. J.; Oliveira, S. EGFR targeted nanobody-photosensitizer conjugates for photodynamic therapy in a pre-clinical model of head and neck cancer. *J. Controlled Release* **2016**, *229*, 93−105.

(14) Muyldermans, S.; Baral, T. N.; Retamozzo, V. C.; De Baetselier, P.; De Genst, E.; Kinne, J.; Leonhardt, H.; Magez, S.; Nguyen, V. K.; Revets, H.; Rothbauer, U.; Stijlemans, B.; Tillib, S.; Wernery, U.; Wyns, L.; Hassanzadeh-Ghassabeh, G.; Saerens, D. Camelid immunoglobulins and nanobody technology. *Vet. Immunol. Immunopathol.* **2009**, *128* (1−3), 178−83.

DOI: 10.1021/acs.molpharmaceut.9b00360
Mol. Pharmaceutics 2019, 16, 3145−3156

(15) Harmsen, M. M.; De Haard, H. J. Properties, production, and applications of camelid single-domain antibody fragments. *Appl. Microbiol. Biotechnol.* **2007**, *77* (1), 13−22.
(16) De Genst, E.; Silence, K.; Decanniere, K.; Conrath, K.; Loris, R.; Kinne, J.; Muyldermans, S.; Wyns, L. Molecular basis for the preferential cleft recognition by dromedary heavy-chain antibodies. *Proc. Natl. Acad. Sci. U. S. A.* **2006**, *103* (12), 4586−91.
(17) De Groof, T. W. M.; Bobkov, V.; Heukers, R.; Smit, M. J. Nanobodies: New avenues for imaging, stabilizing and modulating GPCRs. *Mol. Cell. Endocrinol.* **2019**, *484*, 15−24.
(18) Rosenbaum, D. M.; Rasmussen, S. G.; Kobilka, B. K. The structure and function of G-protein-coupled receptors. *Nature* **2009**, *459* (7245), 356−63.
(19) Kobilka, B. The structural basis of G-protein-coupled receptor signaling (Nobel Lecture). *Angew. Chem., Int. Ed.* **2013**, *52* (25), 6380−8.
(20) Bar-Shavit, R.; Maoz, M.; Kancharla, A.; Nag, J. K.; Agranovich, D.; Grisaru-Granovsky, S.; Uziely, B. G Protein-Coupled Receptors in Cancer. *Int. J. Mol. Sci.* **2016**, *17* (8), 1320.
(21) Dorsam, R. T.; Gutkind, J. S. G-protein-coupled receptors and cancer. *Nat. Rev. Cancer* **2007**, *7* (2), 79−94.
(22) O'Hayre, M.; Degese, M. S.; Gutkind, J. S. Novel insights into G protein and G protein-coupled receptor signaling in cancer. *Curr. Opin. Cell Biol.* **2014**, *27*, 126−35.
(23) O'Hayre, M.; Vazquez-Prado, J.; Kufareva, I.; Stawiski, E. W.; Handel, T. M.; Seshagiri, S.; Gutkind, J. S. The emerging mutational landscape of G proteins and G-protein-coupled receptors in cancer. *Nat. Rev. Cancer* **2013**, *13* (6), 412−24.
(24) Jahnichen, S.; Blanchetot, C.; Maussang, D.; Gonzalez-Pajuelo, M.; Chow, K. Y.; Bosch, L.; De Vrieze, S.; Serruys, B.; Ulrichts, H.; Vandevelde, W.; Saunders, M.; De Haard, H. J.; Schols, D.; Leurs, R.; Vanlandschoot, P.; Verrips, T.; Smit, M. J. CXCR4 nanobodies (VHH-based single variable domains) potently inhibit chemotaxis and HIV-1 replication and mobilize stem cells. *Proc. Natl. Acad. Sci. U. S. A.* **2010**, *107* (47), 20565−70.
(25) de Wit, R. H.; Heukers, R.; Brink, H. J.; Arsova, A.; Maussang, D.; Cutolo, P.; Strubbe, B.; Vischer, H. F.; Bachelerie, F.; Smit, M. J. CXCR4-Specific Nanobodies as Potential Therapeutics for WHIM syndrome. *J. Pharmacol. Exp. Ther.* **2017**, *363* (1), 35−44.
(26) Maussang, D.; Mujic-Delic, A.; Descamps, F. J.; Stortelers, C.; Vanlandschoot, P.; Stigter-van Walsum, M.; Vischer, H. F.; van Roy, M.; Vosjan, M.; Gonzalez-Pajuelo, M.; van Dongen, G. A.; Merchiers, P.; van Rompaey, P.; Smit, M. J. Llama-derived single variable domains (nanobodies) directed against chemokine receptor CXCR7 reduce head and neck cancer cell growth in vivo. *J. Biol. Chem.* **2013**, *288* (41), 29562−72.
(27) Heukers, R.; Fan, T. S.; de Wit, R. H.; van Senten, J. R.; De Groof, T. W. M.; Bebelman, M. P.; Lagerweij, T.; Vieira, J.; de Munnik, S. M.; Smits-de Vries, L.; van Offenbeek, J.; Rahbar, A.; van Hoorick, D.; Soderberg-Naucler, C.; Wurdinger, T.; Leurs, R.; Siderius, M.; Vischer, H. F.; Smit, M. J. The constitutive activity of the virally encoded chemokine receptor US28 accelerates glioblastoma growth. *Oncogene* **2018**, *37* (30), 4110−4121.
(28) Peyrassol, X.; Laeremans, T.; Gouwy, M.; Lahura, V.; Debulpaep, M.; Van Damme, J.; Steyaert, J.; Parmentier, M.; Langer, I. Development by Genetic Immunization of Monovalent Antibodies (Nanobodies) Behaving as Antagonists of the Human ChemR23 Receptor. *J. Immunol.* **2016**, *196* (6), 2893−901.
(29) Scholler, P.; Nevoltris, D.; de Bundel, D.; Bossi, S.; Moreno-Delgado, D.; Rovira, X.; Moller, T. C.; El Moustaine, D.; Mathieu, M.; Blanc, E.; McLean, H.; Dupuis, E.; Mathis, G.; Trinquet, E.; Daniel, H.; Valjent, E.; Baty, D.; Chames, P.; Rondard, P.; Pin, J. P. Allosteric nanobodies uncover a role of hippocampal mGlu2 receptor homodimers in contextual fear consolidation. *Nat. Commun.* **2017**, *8* (1), 1967.
(30) Gandhi, M. K.; Khanna, R. Human cytomegalovirus: clinical aspects, immune regulation, and emerging treatments. *Lancet Infect. Dis.* **2004**, *4* (12), 725−738.
(31) Vischer, H. F.; Siderius, M.; Leurs, R.; Smit, M. J. Herpesvirus-encoded GPCRs: neglected players in inflammatory and proliferative diseases? *Nat. Rev. Drug Discovery* **2014**, *13* (2), 123−39.
(32) Soroceanu, L.; Matlaf, L.; Bezrookove, V.; Harkins, L.; Martinez, R.; Greene, M.; Soteropoulos, P.; Cobbs, C. S. Human cytomegalovirus US28 found in glioblastoma promotes an invasive and angiogenic phenotype. *Cancer Res.* **2011**, *71* (21), 6643−53.
(33) Dziurzynski, K.; Chang, S. M.; Heimberger, A. B.; Kalejta, R. F.; McGregor Dallas, S. R.; Smit, M.; Soroceanu, L.; Cobbs, C. S. Consensus on the role of human cytomegalovirus in glioblastoma. *Neuro Oncol* **2012**, *14* (3), 246−55.
(34) Harkins, L.; Volk, A. L.; Samanta, M.; Mikolaenko, I.; Britt, W. J.; Bland, K. I.; Cobbs, C. S. Specific localisation of human cytomegalovirus nucleic acids and proteins in human colorectal cancer. *Lancet* **2002**, *360* (9345), 1557−63.
(35) Samanta, M.; Harkins, L.; Klemm, K.; Britt, W. J.; Cobbs, C. S. High prevalence of human cytomegalovirus in prostatic intraepithelial neoplasia and prostatic carcinoma. *J. Urol.* **2003**, *170* (3), 998−1002.
(36) Mitchell, D. A.; Xie, W.; Schmittling, R.; Learn, C.; Friedman, A.; McLendon, R. E.; Sampson, J. H. Sensitive detection of human cytomegalovirus in tumors and peripheral blood of patients diagnosed with glioblastoma. *Neuro Oncol* **2008**, *10* (1), 10−8.
(37) Cobbs, C. S.; Harkins, L.; Samanta, M.; Gillespie, G. Y.; Bharara, S.; King, P. H.; Nabors, L. B.; Cobbs, C. G.; Britt, W. J. Human cytomegalovirus infection and expression in human malignant glioma. *Cancer Res.* **2002**, *62* (12), 3347−50.
(38) Scheurer, M. E.; Bondy, M. L.; Aldape, K. D.; Albrecht, T.; El-Zein, R. Detection of human cytomegalovirus in different histological types of gliomas. *Acta Neuropathol.* **2008**, *116* (1), 79−86.
(39) Maussang, D.; Langemeijer, E.; Fitzsimons, C. P.; Stigter-van Walsum, M.; Dijkman, R.; Borg, M. K.; Slinger, E.; Schreiber, A.; Michel, D.; Tensen, C. P.; van Dongen, G. A.; Leurs, R.; Smit, M. J. The human cytomegalovirus-encoded chemokine receptor US28 promotes angiogenesis and tumor formation via cyclooxygenase-2. *Cancer Res.* **2009**, *69* (7), 2861−9.
(40) Maussang, D.; Verzijl, D.; van Walsum, M.; Leurs, R.; Holl, J.; Pleskoff, O.; Michel, D.; van Dongen, G. A.; Smit, M. J. Human cytomegalovirus-encoded chemokine receptor US28 promotes tumorigenesis. *Proc. Natl. Acad. Sci. U. S. A.* **2006**, *103* (35), 13068−73.
(41) Slinger, E.; Maussang, D.; Schreiber, A.; Siderius, M.; Rahbar, A.; Fraile-Ramos, A.; Lira, S. A.; Soderberg-Naucler, C.; Smit, M. J. HCMV-encoded chemokine receptor US28 mediates proliferative signaling through the IL-6-STAT3 axis. *Sci. Signaling* **2010**, *3* (133), ra58.
(42) Kooijmans, S. A.; Aleza, C. G.; Roffler, S. R.; van Solinge, W. W.; Vader, P.; Schiffelers, R. M. Display of GPI-anchored anti-EGFR nanobodies on extracellular vesicles promotes tumour cell targeting. *J. Extracell. Vesicles* **2016**, *5*, 31053.
(43) Goldman, L. A.; Cutrone, E. C.; Kotenko, S. V.; Krause, C. D.; Langer, J. A. Modifications of vectors pEF-BOS, pcDNA1 and pcDNA3 result in improved convenience and expression. *BioTechniques* **1996**, *21* (6), 1013−5.
(44) Casarosa, P.; Menge, W. M.; Minisini, R.; Otto, C.; van Heteren, J.; Jongejan, A.; Timmerman, H.; Moepps, B.; Kirchhoff, F.; Mertens, T.; Smit, M. J.; Leurs, R. Identification of the first nonpeptidergic inverse agonist for a constitutively active viral-encoded G protein-coupled receptor. *J. Biol. Chem.* **2003**, *278* (7), 5172−8.
(45) de Wit, R. H.; Mujic-Delic, A.; van Senten, J. R.; Fraile-Ramos, A.; Siderius, M.; Smit, M. J. Human cytomegalovirus encoded chemokine receptor US28 activates the HIF-1alpha/PKM2 axis in glioblastoma cells. *Oncotarget* **2016**, *7* (42), 67966−67985.
(46) Kim, J.; Mori, T.; Chen, S. L.; Amersi, F. F.; Martinez, S. R.; Kuo, C.; Turner, R. R.; Ye, X.; Bilchik, A. J.; Morton, D. L.; Hoon, D. S. Chemokine receptor CXCR4 expression in patients with melanoma and colorectal cancer liver metastases and the association with disease outcome. *Ann. Surg.* **2006**, *244* (1), 113−20.

DOI: 10.1021/acs.molpharmaceut.9b00360
Mol. Pharmaceutics 2019, 16, 3145−3156

(47) Mukherjee, D.; Zhao, J. The Role of chemokine receptor CXCR4 in breast cancer metastasis. *Am. J. Cancer Res.* **2013**, *3* (1), 46−57.
(48) Kim, J.; Takeuchi, H.; Lam, S. T.; Turner, R. R.; Wang, H. J.; Kuo, C.; Foshag, L.; Bilchik, A. J.; Hoon, D. S. Chemokine receptor CXCR4 expression in colorectal cancer patients increases the risk for recurrence and for poor survival. *J. Clin. Oncol.* **2005**, *23* (12), 2744−53.
(49) Miao, Z.; Luker, K. E.; Summers, B. C.; Berahovich, R.; Bhojani, M. S.; Rehemtulla, A.; Kleer, C. G.; Essner, J. J.; Nasevicius, A.; Luker, G. D.; Howard, M. C.; Schall, T. J. CXCR7 (RDC1) promotes breast and lung tumor growth in vivo and is expressed on tumor-associated vasculature. *Proc. Natl. Acad. Sci. U. S. A.* **2007**, *104* (40), 15735−40.
(50) Hattermann, K.; Held-Feindt, J.; Lucius, R.; Muerkoster, S. S.; Penfold, M. E.; Schall, T. J.; Mentlein, R. The chemokine receptor CXCR7 is highly expressed in human glioma cells and mediates antiapoptotic effects. *Cancer Res.* **2010**, *70* (8), 3299−308.
(51) Bannas, P.; Hambach, J.; Koch-Nolte, F. Nanobodies and Nanobody-Based Human Heavy Chain Antibodies As Antitumor Therapeutics. *Front Immunol* **2017**, *8*, 1603.
(52) Muyldermans, S. Nanobodies: natural single-domain antibodies. *Annu. Rev. Biochem.* **2013**, *82*, 775−97.
(53) Zavrtanik, U.; Lukan, J.; Loris, R.; Lah, J.; Hadzi, S. Structural Basis of Epitope Recognition by Heavy-Chain Camelid Antibodies. *J. Mol. Biol.* **2018**, *430* (21), 4369−4386.
(54) Casarosa, P.; Waldhoer, M.; LiWang, P. J.; Vischer, H. F.; Kledal, T.; Timmerman, H.; Schwartz, T. W.; Smit, M. J.; Leurs, R. CC and CX3C chemokines differentially interact with the N terminus of the human cytomegalovirus-encoded US28 receptor. *J. Biol. Chem.* **2005**, *280* (5), 3275−85.
(55) Cilliers, C.; Liao, J.; Atangcho, L.; Thurber, G. M. Residualization Rates of Near-Infrared Dyes for the Rational Design of Molecular Imaging Agents. *Mol. Imaging Biol.* **2015**, *17* (6), 757−62.
(56) Fraile-Ramos, A.; Kledal, T. N.; Pelchen-Matthews, A.; Bowers, K.; Schwartz, T. W.; Marsh, M. The human cytomegalovirus US28 protein is located in endocytic vesicles and undergoes constitutive endocytosis and recycling. *Mol. Biol. Cell* **2001**, *12* (6), 1737−49.
(57) Juweid, M.; Neumann, R.; Paik, C.; Perez-Bacete, M. J.; Sato, J.; van Osdol, W.; Weinstein, J. N. Micropharmacology of monoclonal antibodies in solid tumors: direct experimental evidence for a binding site barrier. *Cancer Res.* **1992**, *52* (19), 5144−53.
(58) Oliveira, S.; van Dongen, G. A.; Stigter-van Walsum, M.; Roovers, R. C.; Stam, J. C.; Mali, W.; van Diest, P. J.; van Bergen en Henegouwen, P. M. Rapid visualization of human tumor xenografts through optical imaging with a near-infrared fluorescent anti-epidermal growth factor receptor nanobody. *Mol. Imaging* **2012**, *11* (1), 33−46.
(59) Kijanka, M.; Warnders, F. J.; El Khattabi, M.; Lub-de Hooge, M.; van Dam, G. M.; Ntziachristos, V.; de Vries, L.; Oliveira, S.; van Bergen En Henegouwen, P. M. Rapid optical imaging of human breast tumour xenografts using anti-HER2 VHHs site-directly conjugated to IRDye 800CW for image-guided surgery. *Eur. J. Nucl. Med. Mol. Imaging* **2013**, *40* (11), 1718−29.
(60) Beltran Hernandez, I.; Rompen, R.; Rossin, R.; Xenaki, K. T.; Katrukha, E. A.; Nicolay, K.; van Bergen En Henegouwen, P.; Grull, H.; Oliveira, S. Imaging of Tumor Spheroids, Dual-Isotope SPECT, and Autoradiographic Analysis to Assess the Tumor Uptake and Distribution of Different Nanobodies. *Mol. Imaging Biol.* **2019**, DOI: 10.1007/s11307-019-01320-x.
(61) van Tellingen, O.; Yetkin-Arik, B.; de Gooijer, M. C.; Wesseling, P.; Wurdinger, T.; de Vries, H. E. Overcoming the blood-brain tumor barrier for effective glioblastoma treatment. *Drug Resist. Updates* **2015**, *19*, 1−12.
(62) Rissiek, B.; Koch-Nolte, F.; Magnus, T. Nanobodies as modulators of inflammation: potential applications for acute brain injury. *Front Cell Neurosci* **2014**, *8*, 344.
(63) Li, T.; Bourgeois, J. P.; Celli, S.; Glacial, F.; Le Sourd, A. M.; Mecheri, S.; Weksler, B.; Romero, I.; Couraud, P. O.; Rougeon, F.; Lafaye, P. Cell-penetrating anti-GFAP VHH and corresponding fluorescent fusion protein VHH-GFP spontaneously cross the blood-brain barrier and specifically recognize astrocytes: application to brain imaging. *FASEB J.* **2012**, *26* (10), 3969−79.
(64) Li, T.; Vandesquille, M.; Koukouli, F.; Dudeffant, C.; Youssef, I.; Lenormand, P.; Ganneau, C.; Maskos, U.; Czech, C.; Grueninger, F.; Duyckaerts, C.; Dhenain, M.; Bay, S.; Delatour, B.; Lafaye, P. Camelid single-domain antibodies: A versatile tool for in vivo imaging of extracellular and intracellular brain targets. *J. Controlled Release* **2016**, *243*, 1−10.
(65) Bruce, V. J.; Lopez-Islas, M.; McNaughton, B. R. Resurfaced cell-penetrating nanobodies: A potentially general scaffold for intracellularly targeted protein discovery. *Protein Sci.* **2016**, *25* (6), 1129−37.
(66) Quirk, B. J.; Brandal, G.; Donlon, S.; Vera, J. C.; Mang, T. S.; Foy, A. B.; Lew, S. M.; Girotti, A. W.; Jogal, S.; LaViolette, P. S.; Connelly, J. M.; Whelan, H. T. Photodynamic therapy (PDT) for malignant brain tumors–where do we stand? *Photodiagn. Photodyn. Ther.* **2015**, *12* (3), 530−44.
(67) Akimoto, J. Photodynamic Therapy for Malignant Brain Tumors. *Neurol Med. Chir (Tokyo)* **2016**, *56* (4), 151−7.
(68) Slobedman, B.; Mocarski, E. S. Quantitative analysis of latent human cytomegalovirus. *J. Virol* **1999**, *73* (6), 4806−12.
(69) Krishna, B. A.; Spiess, K.; Poole, E. L.; Lau, B.; Voigt, S.; Kledal, T. N.; Rosenkilde, M. M.; Sinclair, J. H. Targeting the latent cytomegalovirus reservoir with an antiviral fusion toxin protein. *Nat. Commun.* **2017**, *8*, 14321.
(70) Zhang, S.; Jia, N.; Shao, P.; Tong, Q.; Xie, X. Q.; Bai, M. Target-selective phototherapy using a ligand-based photosensitizer for type 2 cannabinoid receptor. *Chem. Biol.* **2014**, *21* (3), 338−44.

DOI: 10.1021/acs.molpharmaceut.9b00360
Mol. Pharmaceutics 2019, 16, 3145−3156